Coupled Heat–Mass Transfer CFD–DPM Analysis of a Patented Inertial Separator for Chemical Looping Combustion

Sosnowski Marcin[a], Krzywanski Jaroslaw[b], Grabowska Karolina[c], Zylka Anna[d], Skrobek Dorian[e], Lasek Lukasz[f], Czakiert Tomasz[g], Mirek Pawel[h], Rajczyk Rafal[i]

[a] *Jan Dlugosz University in Czestochowa, Czestochowa, Poland, m.sosnowski@ujd.edu.pl, CA*
[b] *Jan Dlugosz University in Czestochowa, Czestochowa, Poland, j.krzywanski@ujd.edu.pl*
[c] *Jan Dlugosz University in Czestochowa, Czestochowa, Poland, k.grabowska@ujd.edu.pl*
[d] *Jan Dlugosz University in Czestochowa, Czestochowa, Poland, a.zylka@ujd.edu.pl*
[e] *Jan Dlugosz University in Czestochowa, Czestochowa, Poland, d.skrobek@ujd.edu.pl*
[f] *Jan Dlugosz University in Czestochowa, Czestochowa, Poland, l.lasek@ujd.edu.pl*
[g] *Czestochowa University of Technology, Czestochowa, Poland, tomasz.czakiert@pcz.pl*
[h] *Czestochowa University of Technology, Czestochowa, Poland, pawel.mirek@pcz.pl*
[i] *Czestochowa University of Technology, Czestochowa, Poland, rafal.rajczyk@pcz.pl*

Abstract:
Chemical Looping Combustion (CLC) is a promising technology for low- and potentially negative-emission energy conversion, and it constitutes the core scientific context of the MSLimitCO2 project focused on biomass-based CLC. A key component affecting overall process efficiency is the fuel-reactor gas–solid separation and internal recirculation of oxygen carrier and unburned char. This paper addresses a patented cuboidal CLC fuel reactor (Polish Patent PL243901B1) featuring an integrated inertial separator that returns separated solids to the reaction zone, eliminating the need for external carbon-stripping equipment and enabling compact reactor integration. Building on a previously developed and experimentally anchored CFD–DPM framework (validated against pressure measurements on a laboratory test stand), the present study advances the model from “cold” hydrodynamics toward “hot” operation by introducing coupled heat–mass transfer in the separator domain.
The computational approach retains the established modelling backbone (ANSYS Fluent-based CFD with Discrete Phase Model tracking and turbulence closure consistent with earlier work) to preserve comparability of flow structures and separation metrics across operating regimes and design variants. The extension includes solution of the energy equation for the continuous phase and particle thermal balance for the discrete phase, enabling prediction of gas temperature fields, particle temperature histories, and local convective heat exchange rates. Thermal boundary conditions are formulated to represent realistic reactor operation, including heat losses through walls and temperature non-uniformities that can occur near the flue-gas outlet region and within collision/baffle zones characteristic of the patented separator layout.
A parametric analysis is performed for selected separator geometries previously examined via design-point screening, where geometric changes in baffle angles and bulkhead heights were shown to significantly influence particle losses through the flue-gas outlet. The study quantifies how thermal effects modify gas density/viscosity distributions, particle inertia, and near-wall behavior, and how these coupled phenomena translate into changes in separation efficiency and solids return rate under representative hot-flow conditions. The expected outcome is a validated modelling pathway for simultaneous geometric and thermal optimization of the integrated separator, supporting scale-up decisions and design guidelines for CLC systems developed within MSLimitCO2.

Keywords:
Chemical Looping Combustion (CLC); Heat and Mass Transfer; CFD-DPM Coupling; Inertial Separator; Separation Efficiency.

1. Introduction

1.1. Chemical Looping Combustion as a pathway to negative CO_2 emissions

Chemical Looping Combustion (CLC) has emerged as one of the most promising combustion technologies capable of addressing the global demand for energy while simultaneously mitigating greenhouse gas emissions [1]. Unlike conventional combustion processes, CLC employs solid oxygen carriers (OCs), typically transition metal oxides, to transport oxygen from the combustion air directly to the fuel [1]. This cyclic process

is conventionally realized in a dual-reactor system comprising an air reactor and a fuel reactor. In the air reactor, the circulating OC is oxidized by air, whereas in the fuel reactor, the OC is reduced as it provides the lattice oxygen required for fuel oxidation [1]. Because the fuel is kept strictly separated from the nitrogen present in the atmospheric air, the exhaust gas leaving the fuel reactor consists almost exclusively of carbon dioxide (CO_2) and water vapor [2]. Consequently, after the simple condensation of steam, a highly concentrated CO_2 stream is obtained inherently, circumventing the severe energy penalty and high capital costs associated with traditional carbon capture and gas separation units [3].

The integration of the CLC process with renewable solid fuels, such as biomass, unlocks the profound potential of Bioenergy with Carbon Capture and Storage (BECCS) technologies [2]. Since biogenic fuels continuously absorb CO_2 from the atmosphere during their growth phase, utilizing them in a Bio-CLC system ensures that the inherently captured and permanently sequestered carbon dioxide results in net-negative CO_2 emissions [3]. As a result, biomass-based CLC is increasingly recognized as a vital negative emission technology (NET) that will be necessary for meeting stringent international climate targets and achieving global carbon neutrality [2].

The development, scaling, and operational optimization of such advanced negative-emission systems constitute the core scientific focus of the MsLimitCO2 project. Dedicated to the multi-scale investigation of the chemical looping combustion of biomass pellets, the project aims to overcome existing technological barriers related to reactor hydrodynamics, internal recirculation, and complex heat and mass transfer phenomena [4]. Within this comprehensive framework, a profound understanding of both the flow structures and the coupled thermal dynamics is essential for designing highly efficient reactor components that maximize the overall performance of the Bio-CLC process [4].

1.2. The patented fuel reactor with integrated inertial separator

To fully realize the potential of Chemical Looping Combustion (CLC) for solid fuels like biomass, the efficient separation of unburned char and oxygen carrier particles from the exhaust gas stream is of critical importance [5]. In conventional CLC layouts, this gas-solid separation typically relies on extensive external equipment, such as a series of cyclones and dedicated carbon strippers, which capture and return the unreacted solid fuel to the primary reaction zone to ensure complete carbon conversion [6]. However, the inclusion of these external units significantly increases the overall geometric footprint, operational complexity, and capital expenditures of the installation [6].

To address these engineering challenges, an innovative combustion chamber for a fluidized-bed duo-reactor has been developed and protected under Polish Patent No. PL243901B1 [7]. This novel fuel reactor features a compact, cuboidal geometry specifically engineered to optimize spatial utilization while maintaining high fluidization quality and combustion efficiency [7]. The core advancement of this design lies in its integrated inertial separator, which is strategically positioned in the upper section of the reactor, designated as the flue gas outlet zone [5]. The internal separator module incorporates vertical collision bulkhead walls suspended from the chamber's ceiling, beneath which inverted V-shaped baffles are arranged [7].

During operation, the multiphase stream of gases and entrained solids is forced to negotiate this intricate internal geometry. The resulting sharp changes in the flow direction cause the denser solid particles (comprising unburned biomass char and oxygen carriers) to collide with the bulkheads and baffles, subsequently losing their kinetic energy [5]. A sloping internal partition acts as a chute, collecting these separated solids and continuously recirculating them directly back into the fluidized reaction zone [6].

By facilitating this internal recirculation, the patented inertial separator successfully eliminates the necessity for external carbon strippers [6]. Preliminary aerodynamic investigations conducted on a scaled "cold" physical model have demonstrated the high hydrodynamic stability and promising separation potential of this structural configuration [5]. These initial cold-flow experimental findings established a solid foundation for the advanced, multi-scale numerical analyses currently being conducted within the framework of the MsLimitCO2 project.

1.3. From cold to hot model - research gap and motivation

The preliminary phase of the MsLimitCO2 project focused on the purely aerodynamic evaluation of the patented inertial separator. As presented in our previous study at the ECOS2025 conference [4], an isothermal Computational Fluid Dynamics (CFD) coupled with Discrete Phase Modeling (DPM) approach was successfully employed to simulate the "cold" hydrodynamics of the multiphase flow. This baseline model allowed for an extensive parametric screening of the separator’s internal geometry, ultimately identifying an optimal configuration of baffle angles and bulkhead heights that minimized the undesirable escape of solid particles through the flue gas outlet under ambient temperature conditions.

While isothermal ("cold") flow models are recognized as standard and computationally efficient tools for initial aerodynamic design and geometric optimization, they inherently fail to capture the complex multiphase physics of a realistic combustion environment [8]. In actual Chemical Looping Combustion operations, the fuel reactor is subjected to elevated temperatures, typically ranging from 800 °C to 1000 °C. Under such intense thermal conditions, the thermophysical properties of the fluidization gas undergo significant changes, most notably a sharp decrease in gas density and a substantial increase in dynamic viscosity [9]. These temperature-induced

variations directly alter the gas-solid momentum exchange, specifically modifying the drag forces exerted on the particles and shifting the particle Reynolds and Stokes numbers. Consequently, the particle inertia (the primary driving mechanism of the analyzed separator) is heavily impacted, which can lead to flow field alterations and a potential deterioration or shift in the actual separation efficiency compared to ambient conditions.

Therefore, a critical research gap exists in understanding how the coupled phenomena of heat and mass transfer interact with the separator's specific geometry under operating temperatures. The motivation of this current study is to bridge this gap by advancing the previously validated CFD-DPM framework from a "cold" hydrodynamic model to a fully coupled "hot" operational model. By incorporating the continuous-phase energy equation alongside the discrete-phase thermal balance, this study aims to quantitatively evaluate how thermal effects modify flow structures and particle trajectories, thereby providing a robust methodology for the simultaneous geometric and thermal optimization of the CLC fuel reactor.

1.4. Objectives and scope

Building directly upon the theoretical background and the research gaps identified in the previous sections, the primary objective of this study is to formulate and implement a fully coupled heat–mass transfer CFD-DPM framework for the patented inertial separator of the CLC fuel reactor [6]. The overarching goal is to numerically transition the existing, experimentally validated "cold" hydrodynamic model into a comprehensive "hot" operational model that reflects realistic, high-temperature combustion conditions.

To achieve this goal, the specific scope of the presented research encompasses the following tasks:

- Coupling of thermal equations: Extending the established multiphase momentum model by simultaneously solving the energy conservation equation for the continuous fluid phase and the thermal energy balance for the tracked discrete particles;
- Analysis of thermophysical effects: Evaluating how the temperature-induced modifications of the gas phase properties (such as density and dynamic viscosity) affect the particle inertia, gas–solid drag forces, and the ensuing separation performance;
- Geometric re-optimization: Conducting a parametric analysis of selected separator geometries (specifically varying the inverted V-shaped baffle angles and the collision bulkhead heights) to observe how thermal phenomena alter the optimal geometric layouts previously identified in the isothermal studies;
- Cold vs. Hot performance assessment: Providing a direct, quantitative comparison of particle mass flow rates escaping through the flue gas outlet under both ambient and elevated temperatures, quantifying the deviation between the "cold" and "hot" modeling approaches;

Ultimately, the intended outcome of this work is to furnish clear design guidelines and a validated numerical pathway that supports the scaling-up decisions and simultaneous geometric–thermal optimization of the integrated separator within the MsLimitCO2 project framework.

2. Methods

2.1. Governing equations of the continuous phase

In the formulated computational model, the continuous gas phase is described using the Eulerian approach by solving the steady-state Reynolds-Averaged Navier-Stokes (RANS) equations [10]. To accurately capture the non-isothermal phenomena inside the "hot" inertial separator, the previously established hydrodynamic model was expanded to include the conservation of energy. The governing equations for the conservation of mass, momentum, and energy of the fluid phase are expressed as follows.

The mass conservation (continuity) equation is given by:

$$\nabla \cdot (\rho \vec{v}) = S_m \qquad (1)$$

where ρ is the gas density, $\vec{v}$ is the velocity vector, and S_m represents the mass source term resulting from the interaction with the discrete solid phase [10].

The momentum conservation equation is formulated as:

$$\nabla \cdot \left(\rho \overrightarrow{v\vec{v}}\right) = -\nabla p + \nabla \cdot \bar{\bar{\tau}} + \rho \vec{g} + \overrightarrow{F_{DPM}} \qquad (2)$$

where p is the static pressure, $\rho \vec{g}$ is the gravitational body force, and $\overrightarrow{F_{DPM}}$ acts as the momentum sink/source term accounting for the two-way aerodynamic coupling between the gas and the solid particles [11]. The stress tensor $\bar{\bar{\tau}}$ is defined as:

$$\bar{\bar{\tau}} = \mu \left(\left(\nabla \vec{v} + \nabla \overrightarrow{v^T} \right) - \frac{2}{3} \nabla \cdot \vec{v} I \right) \qquad (3)$$

where μ is the dynamic viscosity of the gas, which in the "hot" model varies significantly as a function of temperature, and I is the unit tensor.

To account for the thermal dynamics characteristic of the Chemical Looping Combustion environment, the energy conservation equation is introduced:

$$\nabla \cdot \left(\vec{v}(\rho E + p)\right) = \nabla \cdot \left(k_{eff}\nabla T + \left(\bar{\bar{\tau}}\right\}_{eff} \cdot \vec{v} + S_{h,DPM} \qquad (4)$$

In this equation, E denotes the specific total energy as defined in ANSYS Fluent, combining internal and kinetic energy (the solver employs an enthalpy-based formulation of the energy equation), T is the temperature, and k_{eff} is the effective thermal conductivity [11]. The crucial term $S_{h,DPM}$ denotes the volumetric heat source associated with the interphase convective heat transfer between the continuous gas phase and the discrete solid particles.

To resolve the turbulence within the separator, particularly the complex swirling flows, boundary layer separations, and adverse pressure gradients near the inverted V-shaped baffles and collision bulkheads, the Shear-Stress Transport (SST) $k-\omega$ turbulence model was applied [12]. This model, which blends the robust formulation of the $k-\omega$ model in the near-wall region with the freestream independence of the $k-\epsilon$ model in the far field, has been previously proven to yield highly accurate aerodynamic predictions for this specific reactor geometry.

In the present work, the chemical looping system with ilmenite oxygen carrier is considered only as the thermodynamic background for defining the gas composition and temperature at the separator inlet, while no chemical source terms are activated in the CFD model of the separator.

2.2. Discrete Phase Model — thermal balance of particles

While the continuous gas phase is resolved using the Eulerian framework, the trajectories and thermal histories of the solid particles representing the oxygen carrier and unburned char are simulated using the Lagrangian Discrete Phase Model (DPM) [11]. In the previously developed "cold" model, the tracking of particles relied solely on the balance of aerodynamic and body forces [4]. To transition this framework to "hot" operational conditions, the equations of motion are now fully coupled with the particle thermal balance to capture the convective heat exchange between the phases.

The trajectory of a discrete particle is computed by integrating the force balance equation, which equates the particle inertia with the forces acting on it:

$$\frac{d\vec{v_p}}{dt} = \frac{\vec{v}-\vec{v_p}}{\tau_r} + \vec{g}\frac{\rho_p-\rho}{\rho_p} \qquad (5)$$

where $\vec{v_p}$ is the particle velocity, $\vec{v}$ is the fluid phase velocity, ρ_p is the density of the particle, and ρ is the gas density [11]. The term τ_r represents the particle relaxation time, defined by the drag coefficient C_D and the relative Reynolds number. Because the "hot" conditions significantly decrease the gas density and increase its dynamic viscosity, the drag force and particle inertia are substantially altered, directly influencing the trajectory and separation efficiency.

To account for the non-isothermal conditions within the inertial separator, the particle thermal state is continuously updated along its trajectory by solving the energy balance equation:

$$m_p c_p \frac{dT_p}{dt} = hA_p\left(T_\infty - T_p\right) \qquad (6)$$

where m_p is the mass of the particle, c_p is the particle specific heat capacity, A_p is its surface area, T_p is the current particle temperature, and T_∞ is the local temperature of the continuous gas phase [11].

The convective heat transfer coefficient h is dynamically evaluated throughout the computational domain using the empirical Ranz-Marshall correlation for spherical particles:

$$Nu = \frac{hd_p}{k} = 2.0 + 0.6Re_p^{1/2}Pr^{1/3} \qquad (7)$$

where Nu is the Nusselt number, d_p is the particle diameter, k is the thermal conductivity of the continuous phase, and Pr is the Prandtl number of the gas [13].

This classical correlation was selected because the separator section operates in a relatively dilute, inertia-dominated regime with low local solids volume fractions, where the flow around particles resembles forced convection around isolated spheres. No Sherwood-number-based mass transfer from particles is included in the present non-reactive hot-flow model.

This fully coupled, two-way heat and mass transfer formulation ensures that the thermal energy absorbed or released by the particles is simultaneously manifested as the volumetric heat source term $S_{h,DPM}$ in the energy equation of the continuous phase, accurately replicating the complex thermal physics of the Chemical Looping Combustion system.

2.3. Coupled CFD-DPM heat–mass transfer framework

The accurate simulation of the multiphase environment within the inertial separator requires a robust two-way coupling between the Eulerian gas phase and the Lagrangian discrete particles. In the previously established "cold" model, this coupling was limited strictly to momentum exchange [4]. In the current "hot" model, the numerical framework is expanded to simultaneously account for the interphase exchange of momentum, mass, and thermal energy, reflecting the true operational physics of the Chemical Looping Combustion system.

The interphase momentum transfer, which fundamentally dictates the aerodynamic particle separation, is incorporated into the continuous phase momentum equation through the volumetric source term $\overrightarrow{F_{DPM}}$. This term is computed using the Particle-Source-In-Cell (PSIC) approach by summing the momentum changes of all particles passing through a given computational cell:

$$\overrightarrow{F_{DPM}} = -\frac{1}{V_{cell}}\sum_{i=1}^{N} \dot{m_{p,i}}\Delta\overrightarrow{v_{p,i}} \qquad (8)$$

where V_{cell} is the volume of the computational cell, N is the number of discrete particle streams intersecting the cell, $\dot{m_{p,i}}$ is the mass flow rate of the i-th particle stream, and $\Delta\overrightarrow{v_{p,i}}$ is the change in particle velocity across the cell [14].

Similarly, the convective heat transfer between the high-temperature fluidization gas and the solid particles is aggregated into the continuous phase energy equation via the volumetric heat source term $S_{h,DPM}$:

$$S_{h,DPM} = -\frac{1}{V_{cell}}\sum_{i=1}^{N} \dot{m_{p,i}} c_p \Delta T_{p,i} \qquad (9)$$

where c_p is the specific heat capacity of the solid phase and $\Delta T_{p,i}$ is the change in temperature of the i-th particle stream as it traverses the control volume [11].

This two-way coupling ensures that any localized heating or cooling of the gas phase due to interactions with the particles directly affects the local gas density and dynamic viscosity. Consequently, these temperature-induced alterations in thermophysical properties feed back into the momentum equations, establishing a highly non-linear, interdependent system that dictates the modified separation efficiency under "hot" conditions.

2.4. Research object - modified separator geometry

The primary physical object of this research is the inertial separator module integrated within the patented cuboidal fluidized-bed duo-reactor (Polish Patent No. PL243901B1) [7]. As demonstrated in the preliminary isothermal analyses presented at ECOS2025 Conference [4], the geometric configuration of the inverted V-shaped baffles and the vertical collision bulkhead walls (***Figure 1***) fundamentally determines the separator's operational efficiency [4]. Out of the six original configurations presented in ***Table 1***, Design Point 3 (*DP3*) exhibited the most favorable aerodynamics, yielding the lowest particle loss through the flue gas outlet under ambient conditions [4].

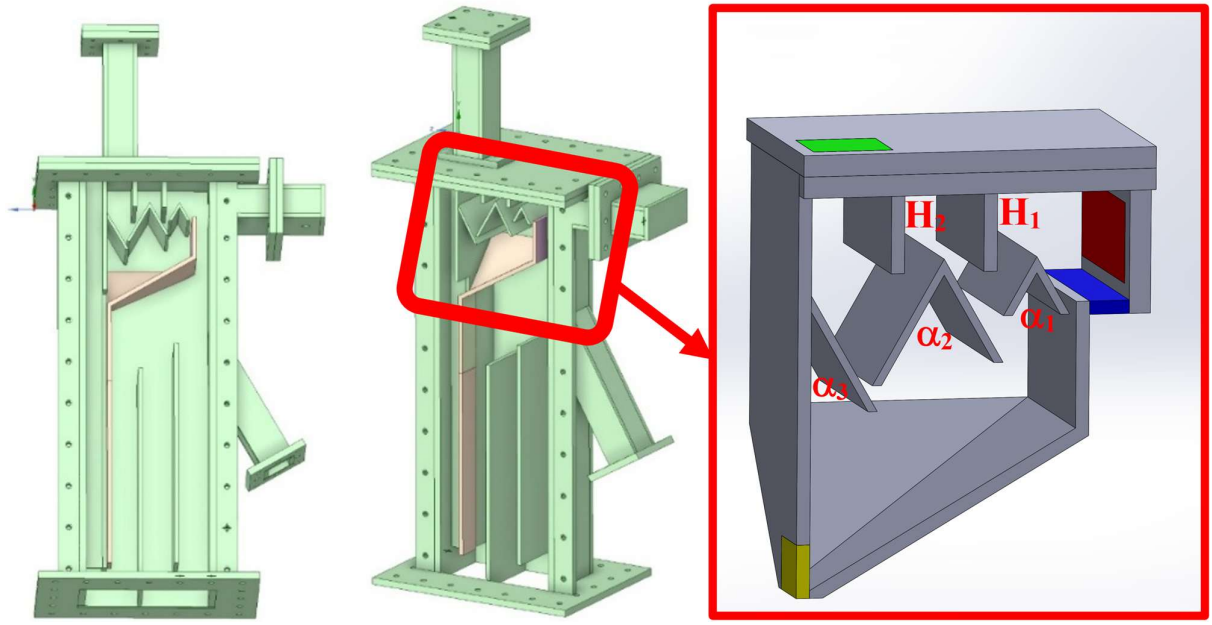

Figure 1. *The 3D model of the fluidized-bed duo-reactor for CLC with the inertial separator indicated in red based on [4].*

Table 1. *Design Points of the analyzed cases*

Design Point	α_1 [°]	α_2 [°]	α_3 [°]	H_1 [mm]	H_2 [mm]
DP1	50	50	25	38	38
DP2	50	50	25	20	20
DP3	60	60	30	38	38
DP4	60	60	30	33	33
DP5	60	60	30	33	38
DP6	60	60	30	38	33

However, to accommodate the thermal alterations in gas density and particle inertia during "hot" operation, the separator geometry for the current study was further refined. Based on the cold-model findings and subsequent Artificial Intelligence (AI) optimization strategies (employing machine learning algorithms such as Random Forests and NSGA-II) developed within the MsLimitCO2 project, the modified geometry implements adjusted baffle inclination angles (*α1*, *α2*, *α3*) and adapted collision bulkhead lengths (*H1*, *H2*). These geometric adjustments are specifically tailored to maintain high solid retention rates despite the increased gas kinematic viscosity and altered drag forces inherent to the elevated operational temperatures. The selected geometric parameters define the computational domain for the subsequent thermo-hydrodynamic simulations.

2.5. Computational domain discretization

The accurate resolution of the highly coupled, thermo-hydrodynamic phenomena occurring within the modified inertial separator relies heavily on the quality of the computational mesh [15]. The 3D computational domain representing the internal volume of the patented fuel reactor (PL243901B1) [7] was discretized using the ANSYS Meshing 2026 R1 software package.

Building upon the successful meshing strategy developed for the isothermal study [4], a similar approach was employed, utilizing high-quality polyhedral volume elements. Polyhedral meshes provide an optimal balance between low numerical diffusion and computational efficiency, significantly accelerating convergence while maintaining the geometrical fidelity of the complex internal baffles and bulkheads [15]. The global minimum and maximum surface mesh element sizes were strictly controlled, maintaining a growth rate of 1.2, while advanced size functions dependent on proximity and curvature were activated to automatically refine the mesh around the critical separation zones.

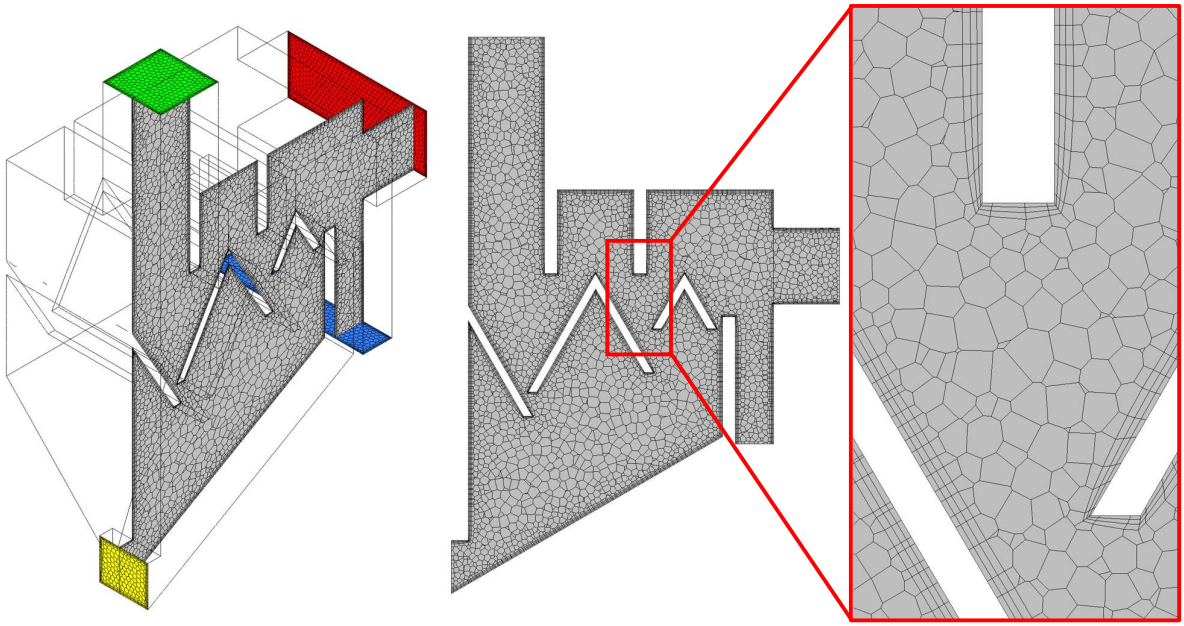

Figure 2. *General view of computational domain discretization using a polyhedral mesh with inflation layers and a detailed view of the inflation layers around the internal baffles.*

Furthermore, because the current "hot" model requires the precise resolution of convective heat transfer between the fluid and the solid boundaries, capturing the thermal and velocity gradients within the boundary layer is of paramount importance. To properly resolve these near-wall phenomena and satisfy the *y+* criteria requisite for the selected *SST k−ω* turbulence model, inflation layers (boundary layer prisms) were introduced adjacent to all solid walls. Three distinct boundary layers were generated with a progressive growth rate of 1.2

and a transition ratio of 0.272, ensuring a smooth volumetric transition from the dense near-wall elements to the polyhedral cells.

The final configuration of the computational mesh was determined through a rigorous mesh independence study. The Grid Convergence Index (GCI) methodology [16], a widely recognized standard in computational fluid dynamics for quantifying numerical uncertainty [17], was applied to ensure that the coupled heat and mass transfer results were insensitive to further grid refinement. The detailed view of the discretized computational domain, highlighting both the internal structures of the separator and the near-wall inflation layers, is depicted in ***Figure 2***. The separator sub-domain analysed in this study has a volume of approximately V_{sep} = 1.135*10^{-3} m³, and the final mesh used for the reported results contains approx. 220k cells.

2.6. Boundary conditions and model setup

The accurate definition of the boundary conditions is a decisive factor governing the reliability of the coupled heat & mass transfer CFD-DPM model. All hydrodynamic boundary conditions applied in the present study were inherited directly from the validated "cold" model [4], ensuring full compatibility and comparability of the results between the isothermal and non-isothermal analyses. The fluidization gas was admitted to the computational domain through the inlet surface at a velocity of 9.43 m/s and a gauge pressure of 1759 Pa, corresponding to the conditions recorded experimentally at the laboratory test stand. Two outlet boundaries were defined: the solids chute (gauge pressure of 1990 Pa) and the flue gas outlet (gauge pressure of 1700 Pa). All remaining surfaces were treated as no-slip solid walls.

To transition the framework from a "cold" to a "hot" model, the thermophysical boundary conditions were introduced in accordance with the characteristic operating temperatures of a biomass-fuelled CLC system. The fluidization gas was defined as a mixture of CO_2 and H_2O representing the actual combustion product composition entering the separator from the fuel reactor, with an inlet temperature representative of the operating range of 900 °C [18]. The temperature-dependent properties of the continuous gas phase - dynamic viscosity $\mu(T)$, thermal conductivity $k(T)$, and specific heat capacity $c_{p,g}(T)$ - were defined using polynomial approximations within the ANSYS Fluent material database [11], enabling the solver to dynamically update these properties throughout the domain in response to local temperature gradients [8].

The discrete solid phase was modelled using the properties of ilmenite ($FeTiO_3$), a natural iron-titanium oxide widely used as an oxygen carrier in CLC research [19]. The particle diameter was set as the Sauter mean diameter of d_p=0.506 mm, with a sphericity of 0.9 and a particle density of ρ_p=2450 kg/m³, consistent with the experimental material used in the cold-model validation [4]. The specific heat capacity of the ilmenite particles was defined as a temperature-dependent property in accordance with values reported in the literature [19]. Particles were injected into the computational domain through the inlet surface, with their initial temperature set equal to the inlet gas temperature, reflecting the fully mixed thermal conditions prevailing at the separator inlet in realistic CLC operation.

Thermal boundary conditions for the solid walls were assigned as a uniform wall temperature, representing the heat loss through the reactor walls to the surroundings [11]. All wall surfaces were also assigned the no-slip condition for the continuous phase, with the *SST k-ω* turbulence model's enhanced wall treatment activated to ensure accurate resolution of both the velocity and thermal boundary layers [12]. The complete numerical setup, including the pressure-velocity coupling scheme (Coupled), the spatial discretization settings (Second Order Upwind for momentum, energy, and turbulence quantities), and the convergence monitors, were preserved consistent with the previously validated model [4], with the sole addition of the energy equation activation and the definition of the particle thermal balance.

2.7. Model validation

The credibility of any computational framework dedicated to resolving complex multiphase and thermal phenomena relies fundamentally on rigorous validation against physical experimental data [20]. The initial baseline version of the present numerical model (restricted to isothermal, "cold" aerodynamic conditions) was comprehensively validated during the primary stages of the MsLimitCO2 project. The physical validation tests were executed on a purpose-built, scaled laboratory test stand of the patented fluidized-bed duo-reactor, utilizing spherical glass beads (ρ_p=2450 kg/m³, d_p=500 µm) to hydrodynamically emulate the behavior of the circulating solid oxygen carriers. During these baseline physical trials, an extensive matrix of operational parameters was continuously recorded, including the mass flow rates of the fluidization gas, total solids inventory, internal pressure distributions across multiple designated measurement points within the reactor, and the crucial mass flow rate of particles successfully entrained into the upper separator section. The computational domain was subsequently subjected to identical boundary conditions. A direct comparison between the experimentally measured static pressure drops across the fluidized bed and the analytically predicted values confirmed a high degree of fidelity. Across all four independent physical test scenarios, the maximum relative error between the experimental data and the numerical predictions generated by the baseline CFD-DPM model did not exceed 10%. This level of agreement solidly corroborates that the selected spatial discretization strategy, the application of the Eulerian-Lagrangian framework, and the implementation

of the *SST k−ω* turbulence model correctly resolve the intricate, swirling gas-solid flow structures navigating the inverted V-shaped baffles and the collision bulkheads.

Building upon this rigorously validated aerodynamic foundation, the present study introduces the non-isothermal ("hot") expansion of the model. By maintaining similar mesh topologies, turbulence closures, and phase-coupling algorithms, while systematically activating the governing equations for energy and temperature-dependent thermophysical properties (as detailed in Sections 2.1. Governing equations of the continuous phase - 2.3. Coupled CFD-DPM heat–mass transfer framework), the aerodynamic validity of the cold model is directly inherited by the hot model [8]. Consequently, the comparative analysis presented in the subsequent sections provides a reliable, physically anchored assessment of how thermal boundary conditions influence particle inertia and alter the geometric separation efficiency of the inertial separator.

3. Results and discussion

3.1. Pressure field distribution for different separator geometries

Figure 3 presents the pressure contours in the separator cross-section for all investigated Design Points (DP1–DP6) under hot-flow conditions. The static pressure level in the lower part of the separator remains close to the solids chute outlet pressure, while the upper regions near the flue-gas outlet and return channel exhibit a gradual pressure decrease towards, consistently reflecting the imposed outlet boundary conditions. This overall trend reproduces the characteristic static pressure stratification previously reported for the cold model, confirming that the introduction of the energy equation does not disturb the macroscopic pressure balance within the system.

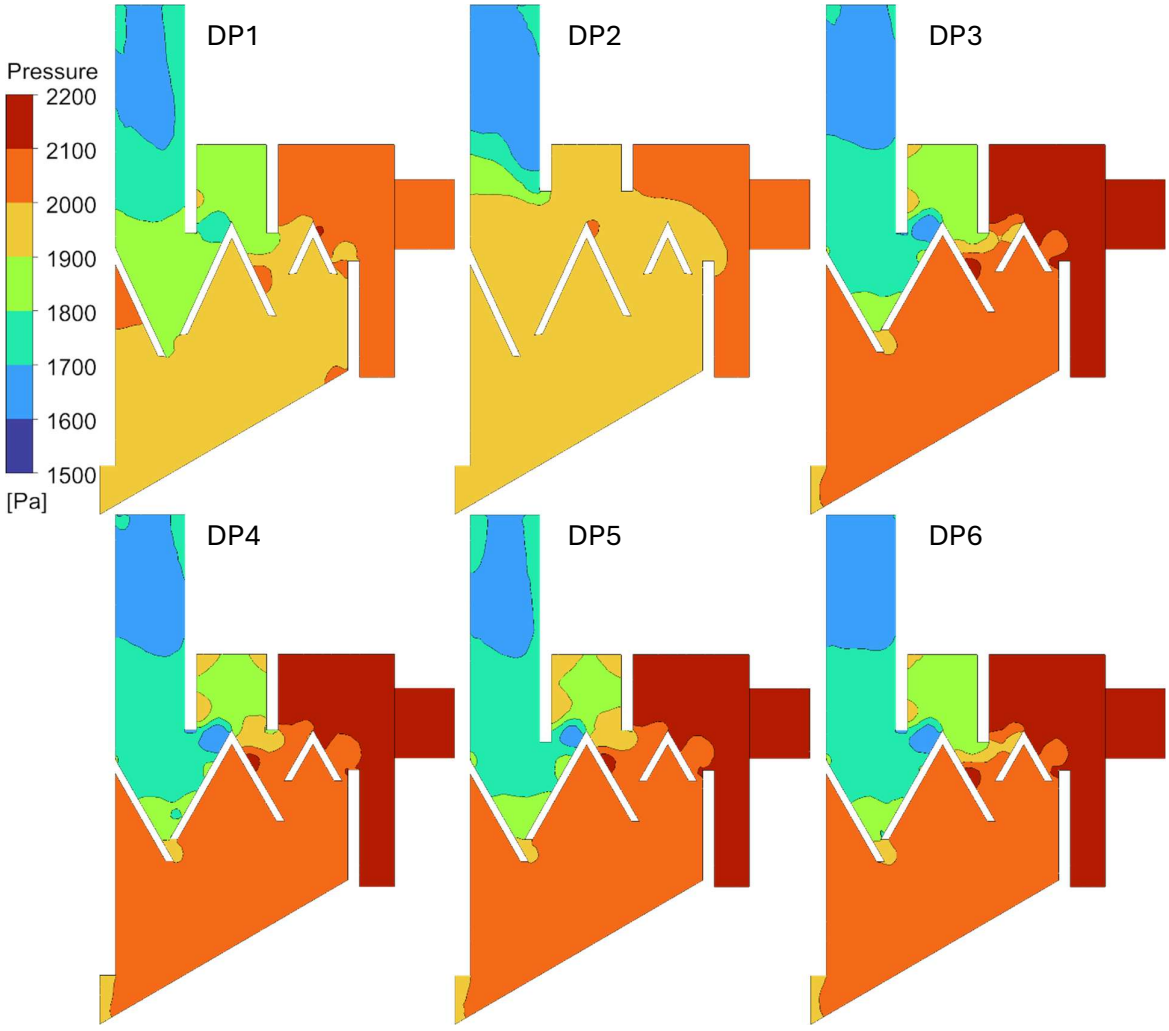

Figure 3. *Pressure contours in the separator cross-section for all investigated Design Points.*

For DP1 and DP2, which employ different collision-wall heights, the pressure field above the first inverted V-shaped baffle exhibits an extended high-pressure region that is weakly separated from the main chamber volume. The pressure gradient between the recirculation chute and the upper flue-gas channel is

comparatively smooth, indicating a less pronounced hydraulic barrier for particle-laden flow. This behavior is consistent with the cold-flow findings, where these configurations were associated with unfavorable flow structures and increased particle escape through the flue-gas outlet.

In contrast, DP3 and DP6, which were previously identified as the most efficient cold-flow geometries, generate a markedly sharper pressure drop across the upper baffle sequence. In these cases, the pressure contours reveal well-defined high-pressure pockets directly downstream of the inclined baffle surfaces and a steeper gradient towards the flue-gas outlet region. Such a distribution promotes the deflection of the gas–solid flow back towards the sloping partition and the solids chute, strengthening the internal recirculation loop. The preservation of this pattern under hot conditions indicates that the geometrical advantages of DP3 and DP6 remain valid even when temperature-dependent changes in gas density and viscosity are taken into account.

DP4 and DP5, characterized by intermediate wall heights and more symmetric baffle layouts, show a pressure field that lies between the extremes described above. The high-pressure zone over the central baffle is more compact than in DP1–DP2, yet the pressure gradient towards the outlet is still gentler than in DP3 and DP6, suggesting a moderate separation performance. Overall, the comparative analysis of the pressure contours confirms that the qualitative ranking of the geometries obtained from cold-flow simulations is preserved under hot operating conditions: configurations DP3 and DP6 generate the most favorable pressure barriers for inertial separation, whereas DP1 and DP2 remain suboptimal from the standpoint of particle retention.

3.2. Gas flow structures and velocity field in the inertial separator

Figure 4 shows the gas streamline patterns colored by the local velocity magnitude for all investigated Design Points (DP1–DP6) under hot-flow conditions. The general flow topology remains qualitatively similar to that reported for the cold model in the previous study, with an accelerating core jet entering the separator from the reactor riser, impingement on the first inverted V-shaped baffle, and subsequent splitting of the flow between the solids-recirculation chute and the flue-gas outlet channel. The maximum gas velocities, exceeding 20 m/s, are consistently observed in the narrow constriction between the riser outlet and the first baffle crest, whereas the lower region above the sloping partition is dominated by slower recirculating motions, which are crucial for enhancing solids residence time and separation.

For DP1 and DP2, the velocity streamlines reveal large, coherent vortical structures extending from the riser outlet into the upper central part of the separator. These strong recirculation cells occupy a substantial portion of the separator height and partially reconnect with the flue-gas outlet leg, which facilitates the entrainment of gas–particle mixtures towards the outlet opening. At the same time, the flow close to the baffle surfaces exhibits limited attachment and weak downward guidance towards the chute, indicating that the relatively short collision walls and less aggressive baffle angles are insufficient to redirect the bulk of the flow towards the return path.

In contrast, DP3 and DP6 generate a markedly more favorable flow pattern, consistent with their superior separation performance identified in both the cold and hot simulations. In these variants, the high-velocity jet leaving the riser is rapidly deflected along the upper surfaces of the first and second baffles, forming a guided channel that bends towards the flue-gas outlet only after passing above the final baffle crest. Below this guided jet, a system of compact recirculation zones develops over the sloping partition and in the vicinity of the baffle, effectively promoting the downward transport of particles towards the chute while limiting their direct exposure to the outlet region. The separation between the high-speed core and the low-velocity recirculation pockets is sharper than in DP1–DP2, which explains the substantially reduced particle losses predicted for DP3 and DP6.

The intermediate configurations DP4 and DP5 exhibit streamline patterns that combine features of both the unfavorable and optimal cases. Although the jet is partially guided along the baffle sequence and a distinct recirculation region develops above the sloping partition, a fraction of the high-velocity stream still penetrates directly towards the outlet channel, particularly over the second baffle. This leak of energetic streamlines into the outlet leg increases the probability of particle entrainment and is consistent with the moderate separation efficiency previously reported for these design points. Overall, the analysis of the streamline maps confirms that the separator geometries that enforce a strong jet deflection combined with well-localized recirculation cells above the partition, namely DP3 and DP6, offer the most robust hydrodynamic conditions for efficient inertial separation under both cold and hot operating regimes.

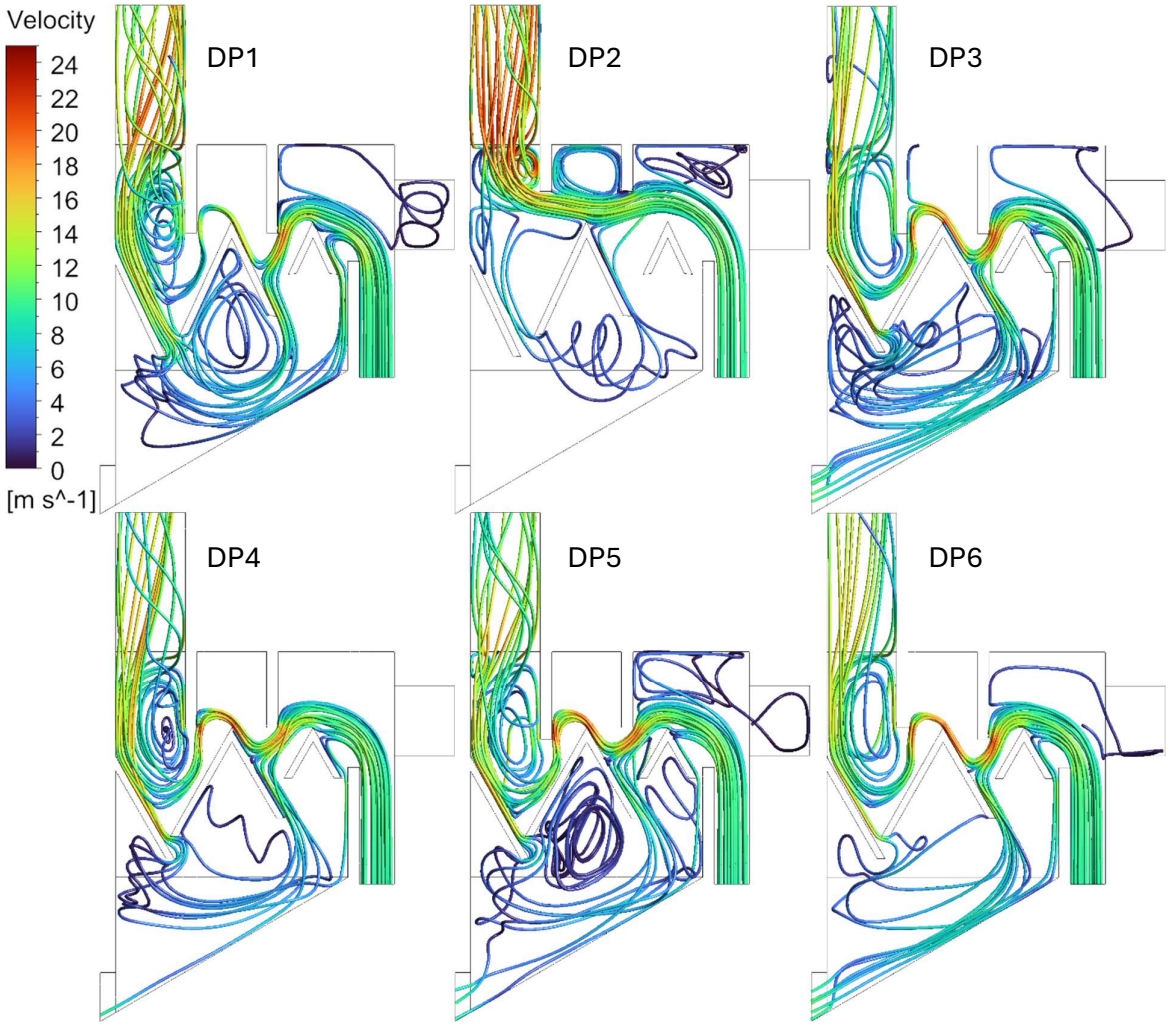

Figure 4. *Gas streamline patterns colored by the local velocity magnitude for all investigated Design Points.*

4. Conclusions

The present work has advanced a previously validated cold-flow CFD-DPM framework of a patented inertial separator integrated into a cuboidal CLC fuel reactor [4] towards a fully coupled heat–mass transfer model representative of hot operating conditions. By solving the energy equation for the continuous phase and the thermal balance for the discrete phase, the model captures temperature-dependent changes in gas properties and their impact on gas–solid momentum and heat exchange within the separator domain.

The pressure and velocity fields obtained for six investigated separator geometries confirm that the overall hydrodynamic behavior of the system remains consistent with earlier isothermal analyses, yet is significantly modulated by thermal effects. Configurations that were previously identified as suboptimal (DP1, DP2) continue to exhibit smooth pressure gradients between the main chamber and the flue-gas outlet and large recirculation zones that partially couple with the outlet leg, thus favoring particle entrainment to the exhaust. In contrast, design points derived from cold-flow and AI-guided optimization (DP3, DP6) preserve strong pressure barriers and favorable streamline guidance that direct the high-velocity jet along the baffle sequence while maintaining compact recirculation pockets above the sloping partition, promoting solids return to the reaction zone.

The coupled hot-flow simulations demonstrate that elevated temperatures, by reducing gas density and increasing viscosity, alter the local drag regime but do not invert the ranking of the considered geometries with respect to separation performance. Geometries analogous to DP3 and DP6 consistently yield the lowest particle escape rates through the flue-gas outlet under both cold and hot conditions, indicating that cold-flow optimization can provide a reliable first approximation for separator design, provided it is subsequently refined by thermo-hydrodynamic modelling. This finding is particularly important for the MsLimitCO2 project, as it validates a multi-stage design strategy in which inexpensive cold-model experiments and simulations are used to narrow down the design space before performing more computationally demanding hot-flow analyses.

The hot-flow simulations also reveal regions of relatively low near-wall velocities in the wake of selected baffles, which may promote solids accumulation and potential deposits in real operation, although such phenomena are not explicitly modelled in the present framework.

The modelling framework developed in this study offers a robust numerical pathway for the simultaneous geometric and thermal optimization of integrated inertial separators in solid-fuel CLC systems. Beyond ranking specific design points, it provides detailed local information on gas–solid interaction, residence time, and heat transfer that can be directly exploited to formulate quantitative design guidelines for future lab and pilot-scale reactors within the MsLimitCO2 project and related CLC applications.

Acknowledgments

The MsLimitCO2 project "Multi-scale investigation of chemical looping combustion of biomass pellets towards negative CO2 emission" (Agreement No. WPC3/2022/44/MSLimitCo2/2024) was funded under the 3rd Polish-Chinese/Chinese-Polish Joint Research Programme operated by the National Centre for Research and Development (NCBR), Poland and the Ministry of Science and Technology (MOST) of the People's Republic of China (National Key R&D Program of China (2024YFE0101400)), and the project No. 2024/08/X/ST8/01676 "Development of guidelines for building computational models of fluidized beds" supported by the National Science Centre, Poland. The support is gratefully acknowledged.

References

[1] Adánez J, Abad A. Chemical-looping combustion: Status and research needs. Proc Combust Inst. 2019;37(4):4303–34.

[2] Mendiara T, García-Labiano F, Abad A, Gayán P, de Diego LF, Izquierdo MT, et al. Negative CO_2 emissions through the use of biofuels in chemical looping technology: A review. Appl Energy. 2018;232:657–84.

[3] Condori S, de Diego LF, García-Labiano F, Gayán P, Abad A, Adánez J. Chemical looping for combustion of solid biomass: A review. Energy Fuels. 2021;35(11):9236–66.

[4] Sosnowski M, Krzywanski J, Grabowska K, Zylka A, Skrobek D, Lasek L, et al. CFD-DPM modeling of mass transfer in the separator of a fuel reactor dedicated to chemical looping combustion. In: Proceedings of the 38th International Conference on Efficiency, Cost, Optimization, Simulation and Environmental Impact of Energy Systems (ECOS); 2025; Paris, France.

[5] Czakiert T, Rajczyk R, Mirek P, Sosnowski M, Krzywanski J, Nowak W. Novel compact fuel reactor for chemical looping combustion of solid fuels. Manuscript prepared within the MsLimitCO2 project framework. Częstochowa: Częstochowa University of Technology; 2024.

[6] Rajczyk R, Czakiert T, Mirek P, Idziak K, Zylka A, Krzywanski J, et al. A novel compact fuel reactor for chemical looping combustion. In: Proceedings of the 7th International Chemical Looping Conference; 2024.

[7] Czakiert T, Krzywański J, Zylka A, Nowak W. Combustion chamber of a fluidized-bed duo-reactor for combustion in a chemical loop. Polish patent PL243901B1. Warsaw: The Patent Office of the Republic of Poland; 2023.

[8] Gimbun M, Chuah JK, Chuah TG, Fakhru'l-Razi A. Investigating the effects of temperature on the performance of novel cyclone separators using large-eddy simulation. Powder Technol. 2023;418:118294.

[9] Wang X, Zhang L, Li S. The effect of temperature on flow field in a cyclone separator by numerical simulation. In: AIChE Spring Meeting and Global Congress on Process Safety; 2019.

[10] Versteeg HK, Malalasekera W. An introduction to computational fluid dynamics: The finite volume method. 2nd ed. Harlow: Pearson Education; 2007.

[11] ANSYS Inc. ANSYS Fluent theory guide. Release 2026 R1. Canonsburg (PA): ANSYS Inc.; 2026.

[12] Menter FR. Two-equation eddy-viscosity turbulence models for engineering applications. AIAA J. 1994;32(8):1598–605.

[13] Ranz WE, Marshall WR. Evaporation from drops. Chem Eng Prog. 1952;48:141–6, 173–80.

[14] Crowe CT, Sharma MP, Stock DE. The particle-source-in cell (PSI-CELL) model for gas-droplet flows. J Fluids Eng. 1977;99(2):325–32.

[15] Sosnowski M, Krzywanski J, Gnatowska R. Polyhedral meshing as an innovative approach to computational domain discretization of a cyclone in a fluidized bed CLC unit. E3S Web Conf. 2017;14:01027.

[16] Celik IB, Ghia U, Roache PJ, Freitas CJ. Procedure for estimation and reporting of uncertainty due to discretization in CFD applications. J Fluids Eng. 2008;130(7):078001.

[17] Krzywanski J., Sztekler K., Szubel M., Siwek T., Nowak W., Mika L. A comprehensive, three-dimensional analysis of a large-scale, multi-fuel, CFB boiler burning coal and syngas. Part 2. Numerical simulations of coal and syngas co-combustion. Entropy 2020; 22 (8), art. no. 856,

[18] Condori S, García-Labiano F, de Diego LF, Izquierdo MT, Abad A, Adánez J. Assessment of the potential of biomass chemical looping combustion for energy production. J Adv Eng Comput. 2025.

[19] Bartocci P, de Diego LF, García-Labiano F, Adánez J, Abad A. Ilmenite: A promising oxygen carrier for the scale-up of chemical looping combustion. Fuel. 2023;338:127324.

[20] Roache PJ. Verification and validation in computational science and engineering. Albuquerque (NM): Hermosa Publishers; 1998